# Comparative Analysis of SNR for Image Sensors with Enhanced Dynamic Range

David X. D. Yang, Abbas El Gamal

Information Systems Laboratory, Stanford University

## ABSTRACT

Dynamic range is a critical figure of merit for image sensors. Often a sensor with higher dynamic range is regarded as higher quality than one with lower dynamic range. For CCD and CMOS sensors operating in the integration mode the sensor SNR monotonically increases with the signal. Therefore, a sensor with higher dynamic range, generally, produces higher quality images than one with lower dynamic range. This, however, is not necessarily the case when dynamic range enhancement schemes are used. For example, using the well capacity adjusting scheme dynamic range is enhanced but at the expense of substantial degradation in SNR. On the other hand, using multiple sampling dynamic range can be enhanced without degrading SNR. Therefore, even if both schemes achieve the same dynamic range the latter can produce higher image quality than the former. The paper provides a quantitative framework for comparing SNR for image sensors with enhanced dynamic range. We introduce a simple model to describe the sensor output response as a function of the photogenerated signal, dark signal, and noise for sensors operating in integration mode with and without dynamic range enhancement schemes. We use the model to quantify and compare dynamic range and SNR for three sensor operation modes, integration with shuttering, using the well capacity adjusting scheme, and using multiple sampling.

**Keywords:** CMOS Image sensor, CCD, Wide Dynamic Range, APS, Pixel level, ADC

## 1. INTRODUCTION

Dynamic range, defined as the ratio of the largest nonsaturating signal to the standard deviation of the noise under dark conditions, is a critical figure of merit for image sensors. It is often regarded as synonymous to sensor quality — a sensor with higher dynamic range is generally believed to produce higher quality images than one with lower dynamic range. Several approaches have been proposed to enhance the dynamic range of a sensor. For CCD and CMOS sensors operating in the integration mode, three such schemes have been proposed: The first is to adjust well capacity during integration, using a lateral overflow gate, to compress the sensor illumination to charge transfer curve.[1,2] The second scheme is to capture multiple samples at different integration times and then to combine the samples to synthesize a high dynamic range image. Nakamura *et al.*[3] describe an implementation of dual sampling using a CMD image sensor. Yadid-Pecht *et al.* [4] describe a clever implementation of dual sampling in a CMOS APS. Yang *et al.*[5] show that pixel level ADC is ideally suited for implementing multiple sampling, since the pixel outputs are available to the ADCs at all times. The third scheme for enhancing dynamic range involves local shuttering .[6] Even though this scheme is conceptually appealing it requires a large number of transistors per pixel to implement, and a considerable amount of post processing to reconstruct the image. For CMOS sensors operating in instantaneous current readout mode,[7,8] a different approach is used. Here the photocurrent is fed into a device with logarithmic response, e.g. a diode connected MOS transistor to compress the sensor transfer curve. Although this scheme can achieve very wide dynamic range, the resulting image quality is generally poor due to low SNR .[8]

In this paper we argue that using dynamic range as a measure of image sensor quality, although well justified for CCD and CMOS sensors operating in the integration mode, can be misleading when dynamic range enhancement schemes are employed. When operating in the integration mode, the sensor signal-to-noise ratio (SNR) monotonically increases with the signal. Therefore, a sensor with higher dynamic range,

Other author information: Email: dyang@isl.stanford.edu, abbas@isl.stanford.edu; Telephone: 650-725-9696; Fax: 650-723-8473

Part of the IS&T/SPIE Conference on Sensors, Cameras, and Systems for Scientific/Industrial Applications • San Jose, California • January 1999
SPIE Vol. 3649 • 0277-786X/99/$10.00

generally, produces higher quality images than one with lower dynamic range. This, however, is not necessarily the case when dynamic range enhancement schemes are used. SNR does not increase monotonically with the signal. For example, using the well capacity adjusting scheme, widening dynamic range comes at the expense of substantial degradation in SNR. On the other hand, the multiple sampling scheme, if properly used, can widen dynamic range without degrading SNR. Therefore, even if both schemes achieve the same dynamic range the latter can produce higher image quality than the former.

The purpose of this paper is to make these arguments clear. To do so we use a simplified model to find the sensor output response as a function of the photogenerated signal, dark signal, and noise for sensors operating in current integration mode with and without dynamic range enhancement schemes. We use the model to quantify dynamic range and SNR for three sensor operation modes. In section 2 we find SNR and dynamic range for a sensor operating in integration mode with shuttering. We show that for a fixed integration time, dynamic range is a good measure of sensor quality. We show that shuttering has little effect on dynamic range and SNR. In section 3 we analyze SNR and dynamic range when the well capacity adjusting scheme is used. In this case we see that as dynamic range is enhanced SNR degrades. In section 4 we analyze dynamic range and SNR when multiple sampling is used. We find that dynamic range can be increased without degradation in SNR.

## 2. DYNAMIC RANGE AND SNR IN THE INTEGRATION MODE

We are concerned with CCD and CMOS image sensors that operate in current integration mode with and without dynamic range enhancement. As depicted in Fig 1, in this mode of operation photocurrent $i_{ph}$ and dark current $i_d$ are integrated on a capacitor, and the accumulated charge is then read out. We assume throughout that both the photocurrent $i_{ph} \geq 0$A, and the dark current $i_d \geq 0$A are constant over integration time*. We also assume that the sensor has a finite charge capacity $q_{max} > 0$ electrons. In Figure 2 we plot the collected charge vs. time for two photocurrent values.

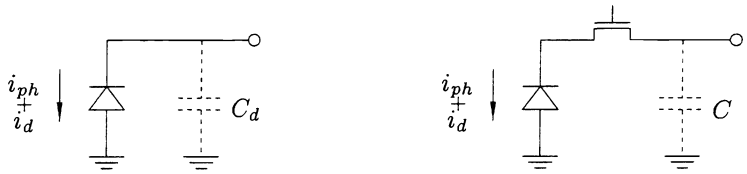


**Figure 1.** Integration mode. The left figure depicts direct integration where current is integrated on the photodiode capacitor. The right figure depicts direct injection, where current is integrated on a separate capacitor.

In this section we introduce a simplified photocurrent to output voltage sensor model, and use it to analyze dynamic range and SNR for sensors operating in integration mode without dynamic range enhancement. In the next two sections we use the same model to analyze dynamic range and SNR when dynamic range enhancement schemes are employed. The model is depicted in Figure 3. The current source $I_s(t)$ represents the shot noise due to photo and dark currents, and is modeled as a white Gaussian noise process with double sided power spectral density $q(i_{ph} + i_d)$. The accumulated charge $Q$ at the end of integration is a functional $f[.]$ of the current $I(t)$ over the integration time $0 \leq t \leq t_{int}$. When the sensor is operating in integration mode without dynamic range enhancement $f[.]$ is simply $min\{\int_0^{t_{int}} I(t)dt, q_{max}\}^\dagger$. Choosing $f[.]$ as a general functional, as we see later, enables us to model the sensor operation when dynamic range enhancement schemes are used.

We assume linear charge-to-voltage amplifier(s) with total amplification $g$. The added charge $Q_r$ represents the noise due to the readout circuits‡, including input referred amplifier noise, and reset noise for

*In the paper, lower case letters will indicate constant values, e.g. mean of a signal, and upper case letters will indicate random variables.

†This assumes that the min is always positive, which is true with high probability, since with high probability the integrated shot noise is much less than the signal charge (including dark current).

‡Quantization noise can also be included in $Q_r$.

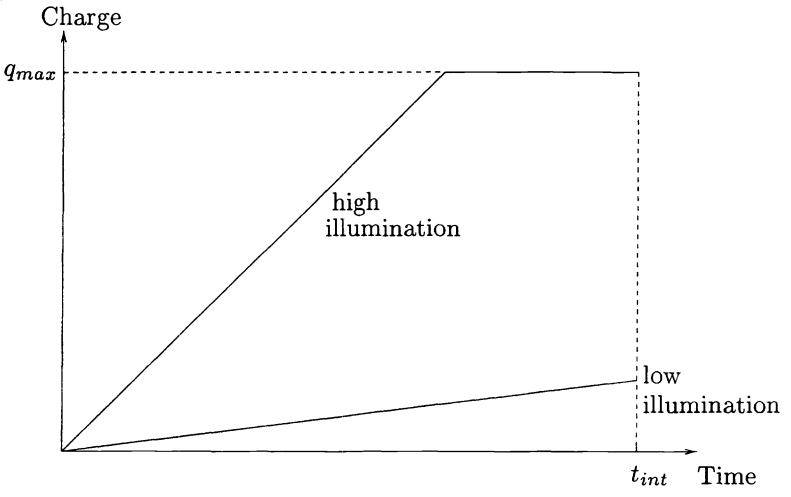


**Figure 2.** Charge collected vs. time.

CMOS APS. We assume that it is zero mean and has average power $\sigma_r^2$. To simplify the model we ignore fixed pattern noise (FPN).

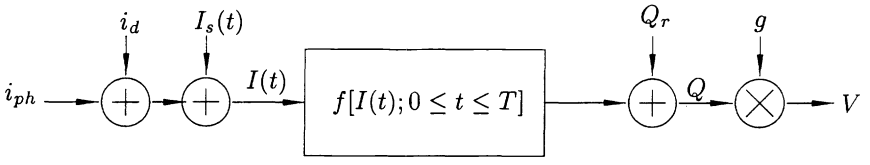


**Figure 3.** Sensor model.

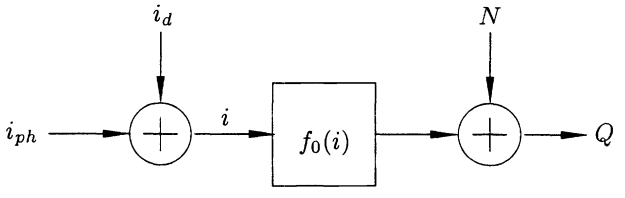


**Figure 4.** Sensor model after combining the noise sources.

Using this model we can now define dynamic range (DR) and signal to noise ratio (SNR). Dynamic range is the ratio of the sensor's largest nonsaturating input signal, i.e. input signal swing, to its smallest detectable input signal. The input signal in our case is the photocurrent $i_{ph}$. For integration time $t_{int}$, the largest nonsaturating input signal is given by, $i_{max} = \frac{q_{max}}{t_{int}} - i_d$. The smallest detectable signal, $i_{min}$, is not as well defined. Clearly, it must be large enough so that it can be discriminated from $i_{ph} = 0$. The convention, which is very optimistic, is to assume that $i_{min}$ is equal to the standard deviation of the input referred noise when no signal is present. To find the standard deviation of the input referred noise we redraw our model as shown in Figure 4. Here the noise is combined into a single zero mean random variable $N$, which is the sum of $Q_r$ and the output referred noise due to shot noise $Q_s$, and $f_0(i) = f[i; 0 \leq t \leq T]$, where $i = i_{ph} + i_d$, i.e. $f[.]$ when $I_s(t) = 0$ for $0 \leq t \leq T$.

For a sensor operating in the integration mode $f_0(i) = min\{it_{int}, q_{max}\}$. This is plotted in Figure 6. Now,

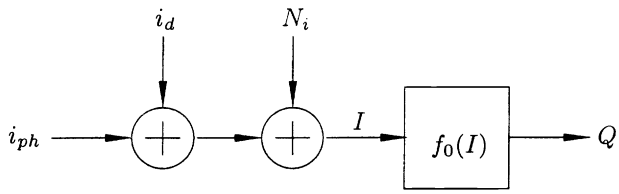


**Figure 5.** Sensor model with input referred noise.

for $i$ sufficiently below $\frac{q_{max}}{t_{int}}$, with high probability, $Q_s = \int_0^{t_{int}} I_s(t)dt$, which has zero mean and variance $q(i_{ph} + i_d)t_{int}$. Since $Q_s$ and $Q_r$ are uncorrelated, the total average noise power $\sigma_Q^2 = q(i_{ph} + i_d)t_{int} + \sigma_r^2$. To find the equivalent zero mean input referred noise $N_i$ we redraw the model again as shown in Figure 5. We assume that $\sigma_{N_i}$ is very small compared to the signal $i$, and therefore $f_0(i + N_i) \approx f_0(i) + N_i f_0'(i)$ evaluated at $i$ (in mean square), provided the derivative exists. Thus, the average power of the equivalent input referred noise

$$\sigma_{N_i}^2 = \frac{\sigma_Q^2}{f_0'(i)^2} = \frac{\sigma_Q^2}{t_{int}^2}.$$

Setting $i_{ph}$ to zero, we get $i_{min} = \frac{1}{t_{int}}\sqrt{qi_d t_{int} + \sigma_r^2}$, and the sensor dynamic range

$$\text{DR} = \frac{i_{max}}{i_{min}} = \frac{q_{max} - i_d t_{int}}{\sqrt{qi_d t_{int} + \sigma_r^2}}. \tag{1}$$

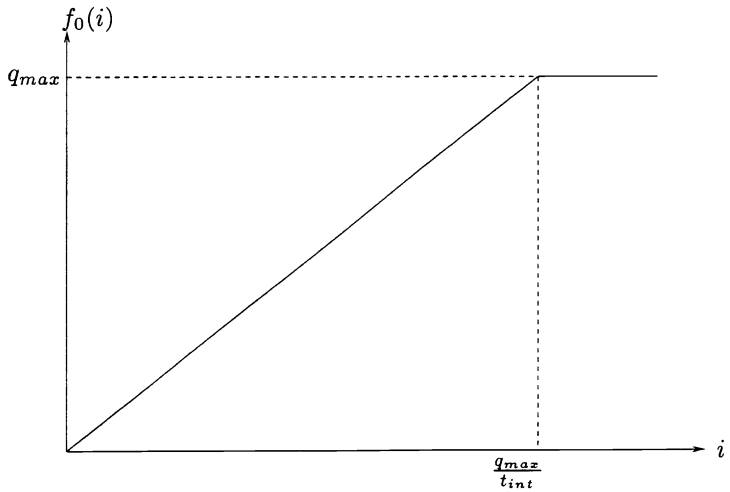


**Figure 6.** $f_0(i)$ vs. $i$.

We define the signal to noise ratio $\text{SNR}(i_{ph})$, which is a function of $i_{ph}$, as the ratio of the input signal power $i_{ph}^2$ to the average input referred noise power $\sigma_{N_i}^2$. For the sensor in integration mode we get

$$\text{SNR}(i_{ph}) = \frac{(i_{ph}t_{int})^2}{q(i_{ph} + i_d)t_{int} + \sigma_r^2}, \text{ for } \quad i_{ph} \leq i_{max}. \tag{2}$$

Note that we do not define SNR for $i_{ph} > i_{max}$, i.e. after the sensor saturates. Of course distortion can be used to extend the SNR definition beyond $i_{max}$ as is customarily done in the ADC literature.[9] Introducing

distortion, however, would complicate our already complex formulas without offering any additional insight. Equation 2 is plotted in Figure 7 for a sensor with $q_{max} = 1.25 \times 10^5$ electrons, $\sigma_r = 20$ electrons, and integration time $t_{int} = 30$ms for three different dark currents $i_d = 1$fA, 5fA, and 15fA. Note that even though the average noise power increases with $i_{ph}$, SNR monotonically increases, first at a rate of 20dBs per decade when read noise dominates, and ultimately at 10dBs per decade as shot noise dominates. Also note that the sensor with the highest dynamic range, i.e. the one corresponding to $i_d = 1$fA, is also the one with the highest SNR. Thus, if we consider SNR to be a good measure of image quality, high dynamic range, which is a single number, can be equally regarded as a good measure of quality. As we will show in the following two sections this is not necessarily the case when dynamic range enhancement schemes are employed.

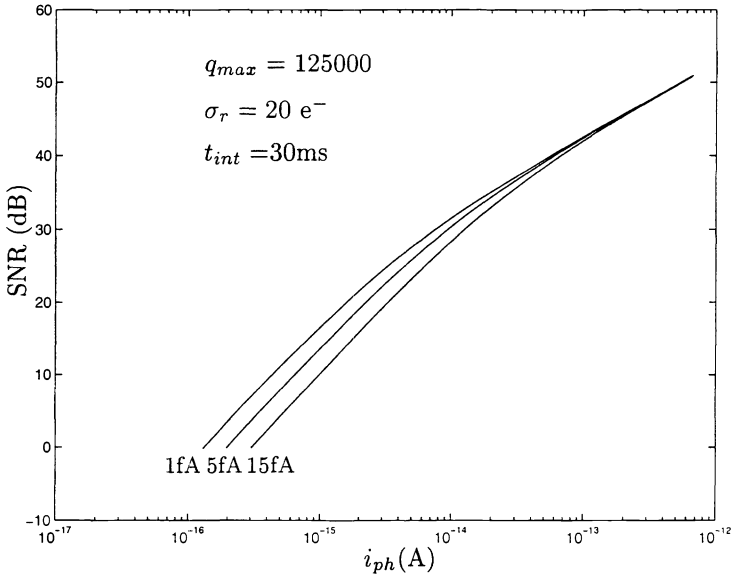


**Figure 7.** SNR vs. $i_{ph}$.

Shuttering is commonly used to adjust integration time to the scene's dynamic range. A fast shutter speed, i.e. short integration time, is used for a bright scene to avoid well saturation, whereas a slow shutter speed is used for a dark scene to increase the image SNR. Equations 1, 2 can be readily used to analyze the effect of shuttering on dynamic range and SNR. For example to find out the effect of shuttering on dynamic range we plot dynamic range vs. integration time $t_{int}$ in Figure 8. For small $t_{int}$, both $i_{min}$ and $i_{max}$ are inversely proportional to $t_{int}$ and dynamic range does not change. For large $t_{int}$, however, dark current $i_d$, decreases $i_{max}$ and its shot noise increases $i_{min}$, resulting in dynamic range roll off. Thus, shuttering does not materially affect a sensor's dynamic range. It merely matches the dynamic range to the scene's range of illumination as illustrated in Figure 9.

## 3. ENHANCING DYNAMIC RANGE BY ADJUSTING WELL CAPACITY

The well capacity adjusting scheme described by Knight[1] and Sayag[2] and implemented by Decker[10] compresses the sensor's current versus charge response curve using a lateral overflow gate, e.g. the reset transistor gate in a CMOS APS. The voltage applied to the overflow gate determines the well capacity. During integration well capacity is monotonically increased to its maximum value. The excess photogenerated charge is drained via the overflow gate. For example, assume that well capacity is adjusted only once at time $t_1$ from $q_{max}\theta$ to full capacity $q_{max}$. Figure 10 plots the average collected charge versus time for two input photocurrent values. Note that when the collected charge reaches $q_{max}\theta$, e.g. the high illumination case in the figure, the output charge is clipped until time $t_1$.

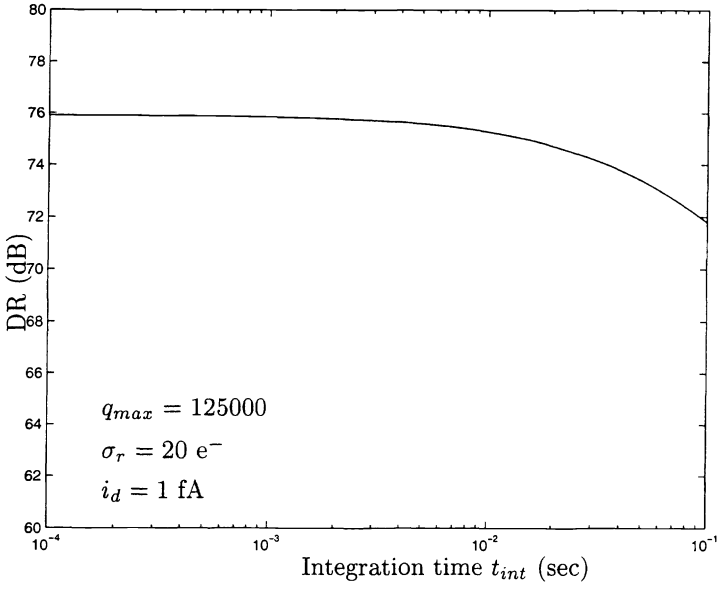


**Figure 8.** Dynamic range vs. integration time $t_{int}$.

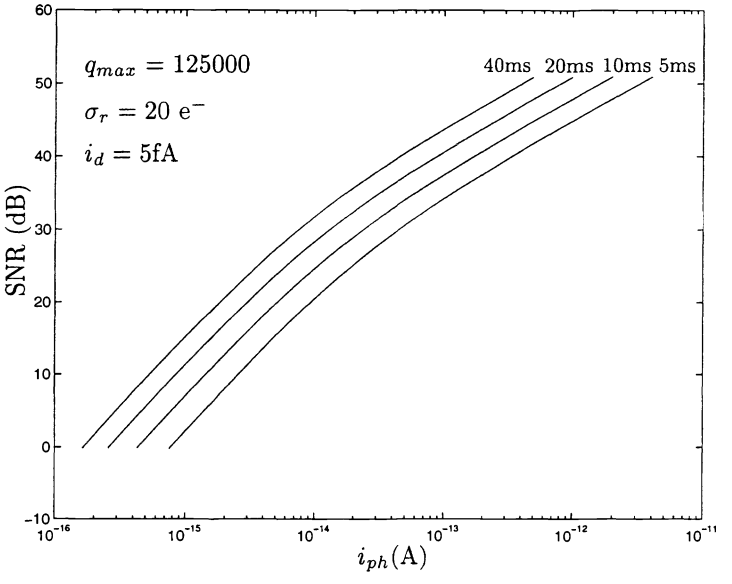


**Figure 9.** SNR vs. $i_{ph}$ at four integration times.

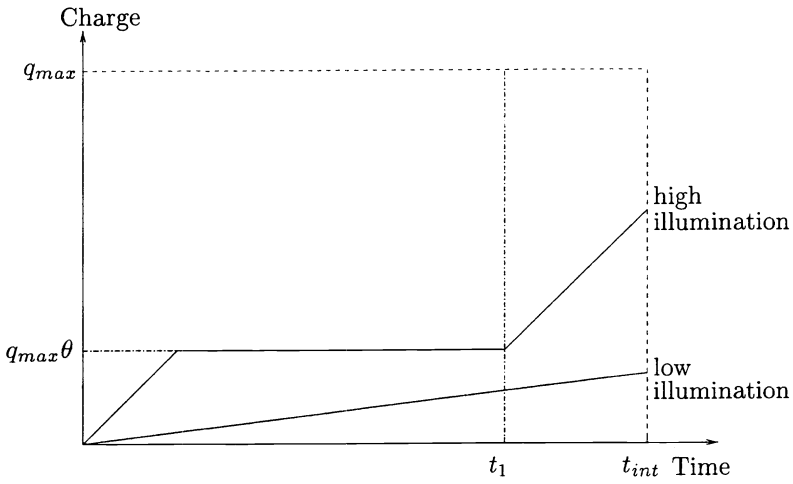


**Figure 10.** Charge vs. time for well capacity adjusting scheme.

In this case the functional in the model

$$f[.] = \begin{cases} \int_0^{t_{int}} I(t)dt & \text{if } 0 \le i_{ph} < \frac{q_{max}\theta}{t_1} - i_d \\ q_{max}\theta + \int_{t_1}^{t_{int}} Idt & \text{if } \frac{q_{max}\theta}{t_1} - i_d \le i_{ph} < \frac{q_{max}(1-\theta)}{t_{int}-t_1} - i_d \\ q_{max} & \text{otherwise.} \end{cases}$$

In order to compute SNR and dynamic range, we need to compute the input referred noise power $\sigma_Q^2$[§]. It is important to note that the input referred noise power is not simply $\frac{\sigma_Q^2}{t_{int}^2}$ since the relationship between $i$ and $Q$ is nonlinear. In this case

$$f_0(i) = \begin{cases} it_{int} & \text{if } i_d \le i < \frac{q_{max}\theta}{t_1} \\ q_{max}\theta + i(t_{int} - t_1) & \text{if } \frac{q_{max}\theta}{t_1} \le i < \frac{q_{max}(1-\theta)}{t_{int}-t_1} \\ q_{max} & \text{otherwise,} \end{cases}$$

This is plotted in Figure 11. Note that the slope decreases beyond $i = i_1 = \frac{q_{max}\theta}{t_1}$, which results in the compression of the response.

It can be easily shown that

$$\sigma_Q^2 = \begin{cases} q(i_{ph} + i_d)t_{int} + \sigma_r^2 & \text{if } 0 \le i_{ph} < \frac{q_{max}\theta}{t_1} - i_d \\ q(i_{ph} + i_d)(t_{int} - t_1) + \sigma_r^2 & \text{if } \frac{q_{max}\theta}{t_1} - i_d \le i_{ph} < \frac{q_{max}(1-\theta)}{t_{int}-t_1} - i_d, \end{cases}$$

and

$$f_0^{'}(i) = \begin{cases} t_{int} & \text{if } i_d \le i < \frac{q_{max}\theta}{t_1} \\ t_{int} - t_1 & \text{if } \frac{q_{max}\theta}{t_1} \le i < \frac{q_{max}(1-\theta)}{t_{int}-t_1} \\ 0 & \text{otherwise.} \end{cases}$$

Therefore

[§]There is an additional noise of $\frac{\kappa}{2}\sqrt{kTC}$ associated with the overflow gate, where $\kappa$ is the subthreshold gate efficiency parameter. This noise can be incorporated in read noise $Q_r$.

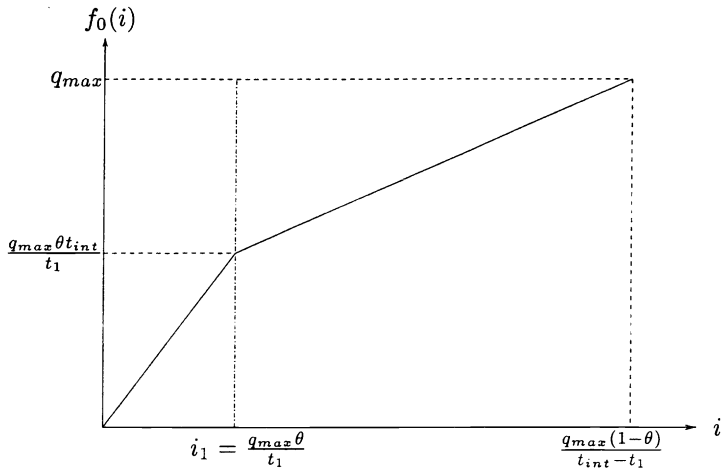


**Figure 11.** $f_0(i)$ vs. $i$ for the well adjusting scheme.

$$\mathrm{SNR}(i_{ph}) = \begin{cases} \frac{i_{ph}^2 t_{int}^2}{q(i_{ph}+i_d)t_{int}+\sigma_r^2} & \text{if } 0 \le i_{ph} < \frac{q_{max}\theta}{t_1} - i_d \\ \frac{i_{ph}^2 (t_{int}-t_1)^2}{q(i_{ph}+i_d)(t_{int}-t_1)+\sigma_r^2} & \text{if } \frac{q_{max}\theta}{t_1} - i_d \le i_{ph} < \frac{q_{max}(1-\theta)}{t_{int}-t_1} - i_d. \end{cases}$$

Now, $i_{max} = \frac{q_{max}(1-\theta)}{t_{int}-t_1} - i_d$, and $i_{min}$ is the same as before. Thus, for small $i_d$, dynamic range is enhanced by a factor

$$\mathrm{DRF} = \frac{1-\theta}{1-\frac{t_1}{t_{int}}}.$$

At $i_1$, assuming that shot noise dominates, $\mathrm{SNR}(i_{ph})$ dips by a factor

$$\mathrm{DIP} = (1 - \frac{t_1}{t_{int}}),$$

which is inversely proportional to the dynamic range enhancement factor DRF. This is illustrated in Figure 12, where SNR is plotted versus $i_{ph}$ using the same sensor parameters as before, and assuming that $i_d = 1\mathrm{fA}$, $\theta = \frac{7}{8}$, and $\frac{t_1}{t_{int}} = \frac{255}{256}$. In this case DRF$\approx 32$, and DIP$\approx \frac{1}{256}$, i.e. around 24 dBs.

The analysis can be extended to any number of well capacity adjustments $k$. In this case let $0 < \theta_i < 1$, $1 \le i \le k$ be the resulting fractions of the well capacity corresponding to the adjustments, and $0 < t_i < t_{int}$, be the adjustment times. It can be shown that dynamic range expands by

$$\mathrm{DRF} = \frac{\frac{q_{max}(1-\theta_k)}{t_{int}-t_k} - i_d}{\frac{q_{max}}{t_{int}} - i_d} \approx \frac{1-\theta_k}{1-\frac{t_k}{t_{int}}},$$

and

$$\mathrm{SNR}(i_{ph}) = \begin{cases} \frac{i_{ph}^2 (t_{int}-t_0)^2}{q(i_{ph}+i_d)(t_{int}-t_0)+\sigma_r^2} & \text{if } 0 \le i_{ph} < \frac{q_{max}\theta_1}{t_1-t_0} - i_d \\ \frac{i_{ph}^2 (t_{int}-t_1)^2}{q(i_{ph}+i_d)(t_{int}-t_1)+\sigma_r^2} & \text{if } \frac{q_{max}(\theta_1-\theta_0)}{t_1-t_0} - i_d \le i_{ph} < \frac{q_{max}(\theta_2-\theta_1)}{(t_2-t_1)} - i_d \\ \vdots & \\ \frac{i_{ph}^2 (t_{int}-t_{k-1})^2}{q(i_{ph}+i_d)(t_{int}-t_{k-1})+\sigma_r^2} & \text{if } \frac{q_{max}(\theta_{k-1}-\theta_{k-2})}{t_{k-1}-t_{k-2}} - i_d \le i_{ph} < \frac{q_{max}(\theta_k-\theta_{k-1})}{t_k-t_{k-1}} - i_d \\ \frac{i_{ph}^2 (t_{int}-t_k)^2}{q(i_{ph}+i_d)(t_{int}-t_k)+\sigma_r^2} & \text{if } \frac{q_{max}(\theta_k-\theta_{k-1})}{t_k-t_{k-1}} - i_d \le i_{ph} < \frac{q_{max}(1-\theta_k)}{t_{int}-t_k} - i_d. \end{cases}$$

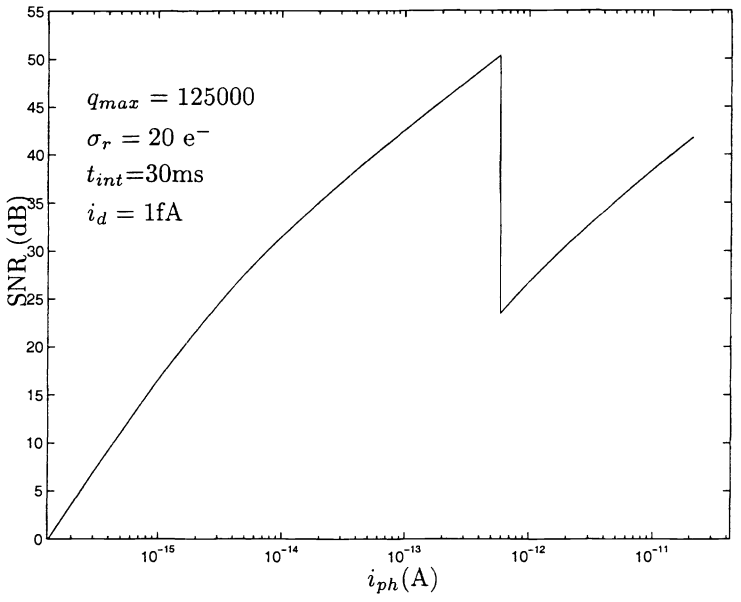


**Figure 12.** SNR vs. $i_{ph}$ for the well capacity adjustment scheme. Dynamic range is enhanced by a factor of 32

Note that as dynamic range is increased, the final SNR($i_{max}$) degrades by the same factor $1-\theta_k$ relative to peak SNR when no dynamic range enhancement is used. Moreover, the sum of the SNR dips, expressed in dBs, is approximately $|10\log_{10}(1-\frac{t_k}{t_{int}})|$, which is always greater than DRF expressed in dBs. In particular the difference, expressed in dBs, between the sum of the SNR dips and half of DRF is equal to the SNR($i_{max}$) degradation factor expressed in dBs.

In Figure 13 we plot SNR versus $i_{ph}$ for $k=8$ capacity adjustments. The capacity levels $\theta_i = \frac{i}{10}$ and adjustment times $t_i = 1-\frac{1}{10*2^{i-1}}$ for $i=1,2,\ldots,8$ are chosen so that the resulting average charge $f_0(.)$ vs. $i_{ph}$ curve assumes an *A-law* companding shape. Dynamic range is increased by DRF$\approx$ 256, i.e. 48 dB. The sum of the SNR dips is $\approx$ 31dBs, and the SNR($i_{max}$) degrades by 7dBs.

## 4. ENHANCING DYNAMIC RANGE VIA MULTIPLE SAMPLING

Dual sampling has been used to enhance the dynamic range for CCD sensors, CMD sensors,[3] and CMOS APS sesnors.[4] A scene is imaged twice, once after a short integration time and another after a much longer integration time, and the two images are combined into a high dynamic range image. Conceptually, the short integration time image captures the high illumination areas before the well saturates and the long integration time image captures the low illumination areas after adequate integration time. Two images, however, may not be sufficient to represent the areas of the scene that are too dark to be captured in the first image and too bright to be captured in the second. Yang *et al.*[5] show that pixel level ADC is ideally suited for implementing multiple sampling in general. The paper considers the implementation of multiple sampling for an exponentially increasing integration times. In this case, dynamic range is enhanced by a factor of $2^k$ and the combined image has a floating point resolution with exponent $k$.

In this section we use our sensor model to analyze SNR and dynamic range when multiple sampling is used. We first investigate dual sampling at $\frac{t_{int}}{a}$ and $t_{int}$, for $a>1$. Figure 14 plots the average collected charge versus time for three illuminations. Note that by sampling at $\frac{t_{int}}{a}$, the moderate illumination signal can be sampled before the sensor saturates.

For dual sampling it can be shown that the functional in our model

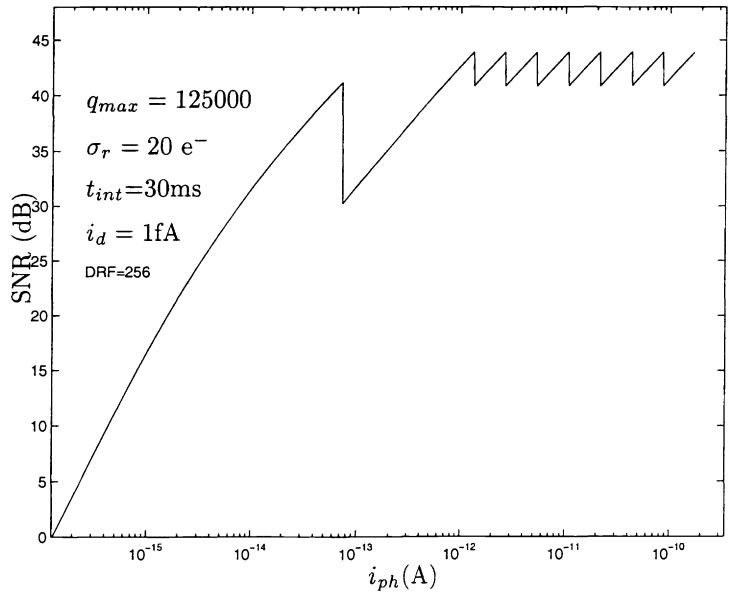


**Figure 13.** SNR vs. $i_{ph}$ for the well capacity adjustment scheme. Dynamic range is enhanced by a factor of 256

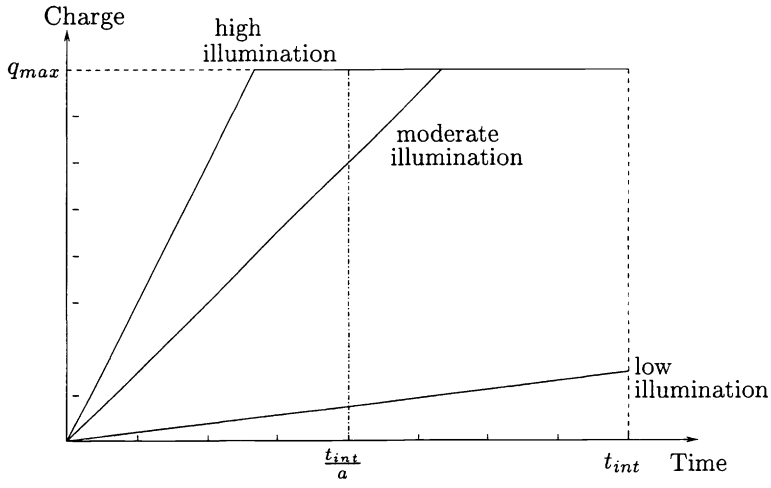


**Figure 14.** Charge vs. time for dual sampling.

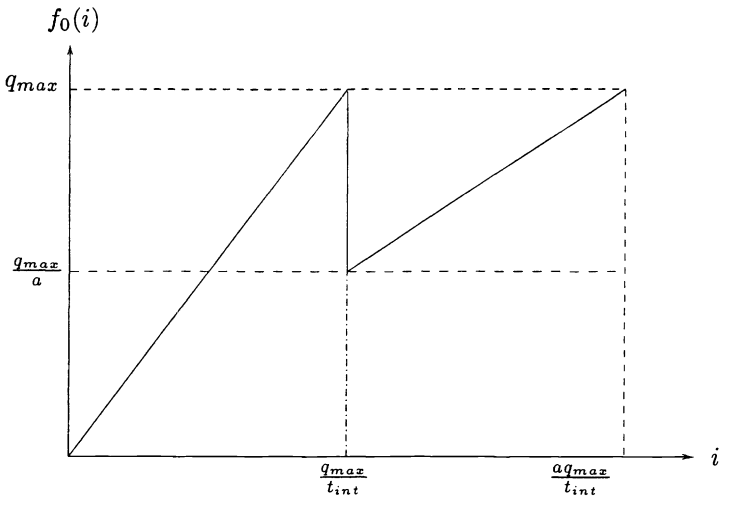


**Figure 15.** $f_0(i)$ vs. $i$ for dual sampling.

$$f[.] = \begin{cases} \int_0^{t_{int}} I(t)dt & \text{if } 0 \le i_{ph} < \frac{q_{max}}{t_{int}} - i_d \\ \int_0^{\frac{t_{int}}{a}} I(t)dt & \text{if } \frac{q_{max}}{t_{int}} - i_d \le i_{ph} < \frac{aq_{max}}{t_{int}} - i_d, \\ q_{max} & \text{otherwise,} \end{cases}$$

and

$$f_0(i) = \begin{cases} it_{int} & \text{if } i_d \le i < \frac{q_{max}}{t_{int}} \\ \frac{it_{int}}{a} & \text{if } \frac{q_{max}}{t_{int}} \le i < \frac{aq_{max}}{t_{int}} \\ q_{max} & \text{otherwise.} \end{cases}$$

Figure 15 plots $f_0(i)$ versus $i$. Note that, unlike the previous cases, $f_0(.)$ is not a one-to-one function. The average noise power

$$\sigma_Q^2 = \begin{cases} q(i_{ph} + i_d)t_{int} + \sigma_r^2 & \text{if } 0 \le i_{ph} < \frac{q_{max}}{t_{int}} - i_d \\ q(i_{ph} + i_d)\frac{t_{int}}{a} + \sigma_r^2 & \text{if } \frac{q_{max}}{t_{int}} - i_d \le i_{ph} < \frac{aq_{max}}{t_{int}} - i_d. \end{cases}$$

We can now compute

$$\text{SNR}(i_{ph}) = \begin{cases} \frac{i_{ph}^2 t_{int}^2}{q(i_{ph}+i_d)t_{int}+\sigma_r^2} & \text{if } 0 \le i_{ph} < \frac{q_{max}}{t_{int}} - i_d \\ \frac{i_{ph}^2 (\frac{t_{int}}{a})^2}{q(i_{ph}+i_d)\frac{t_{int}}{a}+\sigma_r^2} & \text{if } \frac{q_{max}}{t_{int}} - i_d \le i_{ph} < \frac{aq_{max}}{t_{int}} - i_d. \end{cases}$$

Since $i_{max} = \frac{aq_{max}}{t_{int}} - i_d$ and $i_{min}$ is the same as before, the dynamic range enhancement factor

$$\text{DRF} = \frac{\frac{aq_{max}}{t_{int}} - i_d}{\frac{q_{max}}{t_{int}} - i_d} \approx a, \quad \text{for small } i_d.$$

As in the case of well capacity adjusting, SNR dips in the middle. For the same DRF, however, the dip is smaller. Moreover, the final SNR($i_{max}$) is always equal to the peak SNR without dynamic range enhancement.

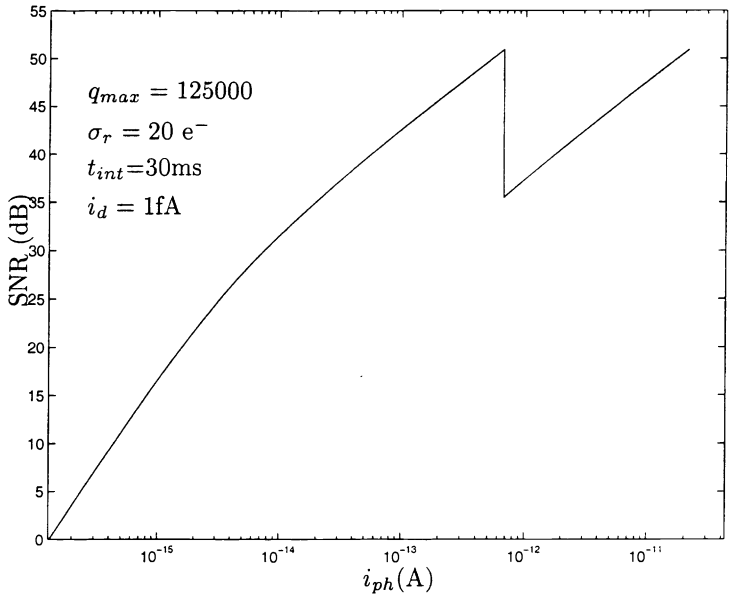


**Figure 16.** SNR vs. $i_{ph}$ example for the dual sampling. Dynamic range is enhanced by a factor of 32.

Figure 16 plots SNR vs. $i_{ph}$ for $a = 32$, $t_{int} = 30$ms, and assuming the same sensor parameter values as before.

The analysis can be extended to multiple sampling in general. For $k+1$ samples at $\frac{t_{int}}{2^k}$, $\frac{t_{int}}{2^{k-1}}$, ..., $\frac{t_{int}}{2}$, $t_{int}$), we get

$$\text{DRF} = \frac{\frac{2^k q_{max}}{t_{int}} - i_d}{\frac{q_{max}}{t_{int}} - i_d} \approx 2^k,$$

and

$$\text{SNR}(i_{ph}) = \begin{cases} \frac{i_{ph}^2 t_{int}^2}{q(i_{ph}+i_d)t_{int}+\sigma_r^2} & \text{if } 0 \le i_{ph} < \frac{q_{max}}{t_{int}} - i_d \\ \frac{i_{ph}^2 (t_{int}/2)^2}{q(i_{ph}+i_d)t_{int}/2+\sigma_r^2} & \text{if } \frac{q_{max}}{t_{int}} - i_d \le i_{ph} < \frac{2q_{max}}{t_{int}} - i_d \\ \vdots & \vdots \\ \frac{i_{ph}^2 (t_{int}/2^{k-1})^2}{q(i_{ph}+i_d)t_{int}/2^{k-1}+\sigma_r^2} & \text{if } \frac{2^{k-2}q_{max}}{t_{int}} - i_d \le i_{ph} < \frac{2^{k-1}q_{max}}{t_{int}} - i_d \\ \frac{i_{ph}^2 (t_{int}/2^k)^2}{q(i_{ph}+i_d)t_{int}/2^k+\sigma_r^2} & \text{if } \frac{2^{k-1}q_{max}}{t_{int}} - i_d \le i_{ph} < \frac{2^k q_{max}}{t_{int}} - i_d. \end{cases}$$

This is plotted in Figure 17 for $k = 8$ and assuming $t_{int} = 30$ms, and the sensor parameter values in the previous examples. Dynamic range is enhanced by DRF$\approx$ 256 as expected.

## 5. CONCLUSION

We have shown that using the well adjusting scheme SNR degrades as dynamic range is increased. On the other hand using the multiple sampling scheme, dynamic range can be widened without degrading SNR. To demonstrate this, in Figure 18 we compare the case of a single well capacity adjustment to dual sampling by combining the SNR vs. $i_{ph}$ plots for the examples in Figures 12, and 16. Both schemes achieve DRF= 32. Dual sampling, however, exhibits better SNR for large $i_{ph}$s.

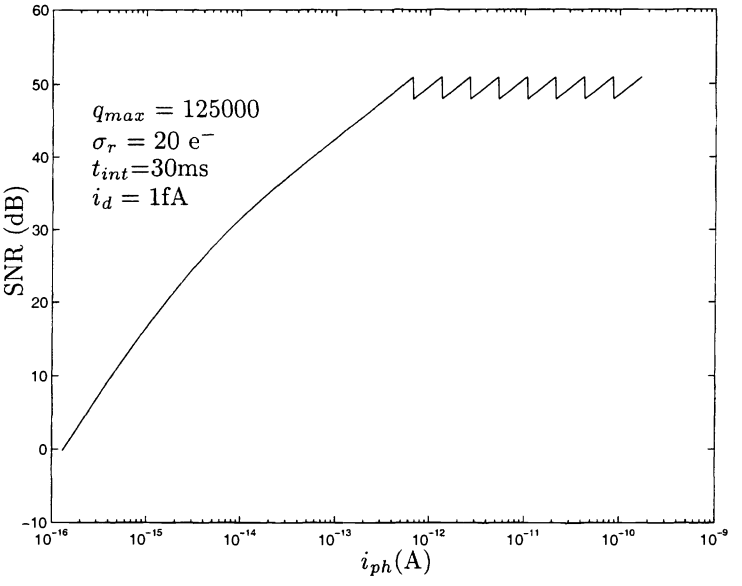


**Figure 17.** SNR vs. $i_{ph}$ example for multiple sampling. Dynamic range is enhanced by a factor of 256.

In Figure 19 we compare well capacity adjusting to multiple sampling by combining the plots of the examples in Figures 13 and 17. Both schemes achieve DRF= 256. Note that multiple sampling achieves around 10dBs higher SNR. Moreover, the SNR for the well adjusting scheme dips by more than 10dB in the middle. This clearly demonstrates that multiple sampling enjoys better SNR than well capacity adjustment at the same DRF. In fact if we include fixed pattern noise, well barrier thermal noise and quantization noise in our analysis, it can be shown that the difference in SNR in favor of multiple sampling is even greater.

In the paper We used the SNR plots to compare the different schemes. Often, it is more convenient to use a single SNR number instead. This can be done by computing an average SNR with respect to the desired illumination probability density function $p_{i_{ph}}(.)$, $\overline{\text{SNR}} = \int \text{SNR}(i_{ph}) p_{i_{ph}}(i_{ph}) di_{ph}$. The plot, of course, provides a more complete description of SNR.

In our definition of dynamic range $i_{min}$ is the standard deviation of the noise under dark conditions. If we use SNR as a measure of image quality, this definition is very optimistic. SNR around $i_{min}$ is close to zero dB, which clearly results in unacceptable image quality. In this case it is more appropriate to define a minimum acceptable SNR for image quality. For example if we define the minimum acceptable SNR to be 20dB, dynamic range may be severly reduced as demontrated in Figure 20 which plots SNR vs. $i_{ph}$ for single well capacity adjustment scheme. Here dynamic range drops from 104dB to 83dB.

The sensor model introduced in this paper proved useful in formalizing the definitions of dynamic range and SNR. This model is general enough to describe sensor nonlinearity, and other potential dynamic range enhancement schemes by properly defining the functional $f[.]$. The model can also be readily extended to include FPN and input illumination that varies during integration.

## ACKNOWLEDGEMENTS

The work reported in this paper was partially supported under the Programmable Digital Camera Program by Intel, HP, Kodak, Interval Research, and Canon, and by ADI.

## REFERENCES

1. T. F. Knight, *Design of an Integrated Optical Sensor with On-Chip Preprocessing.* PhD thesis, MIT, 1983.

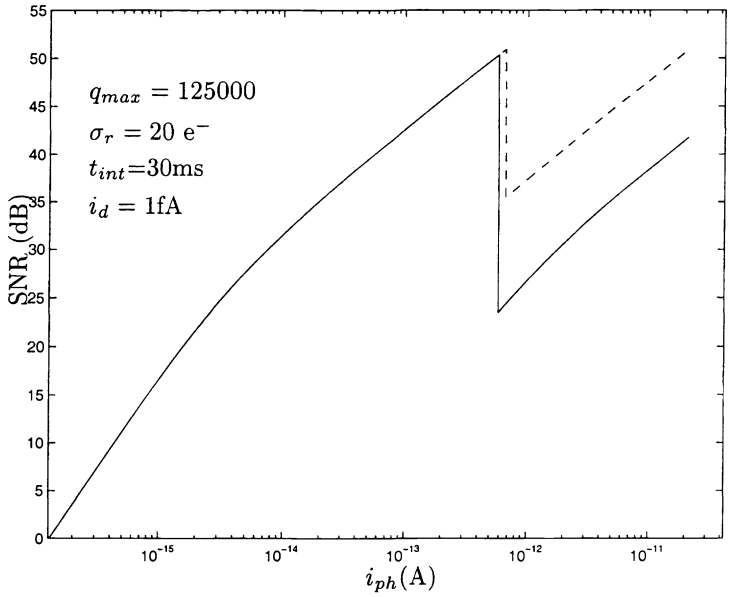


**Figure 18.** SNR vs. $i_{ph}$ for both well capacity adjustment and dual sampling. DRF = 32

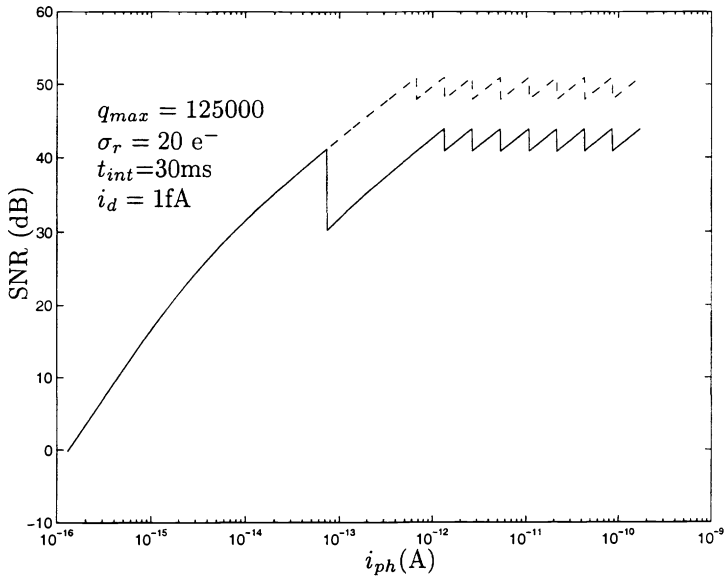


**Figure 19.** SNR vs. $i_{ph}$ for both well capacity adjustment and multiple sampling. DFR = 256

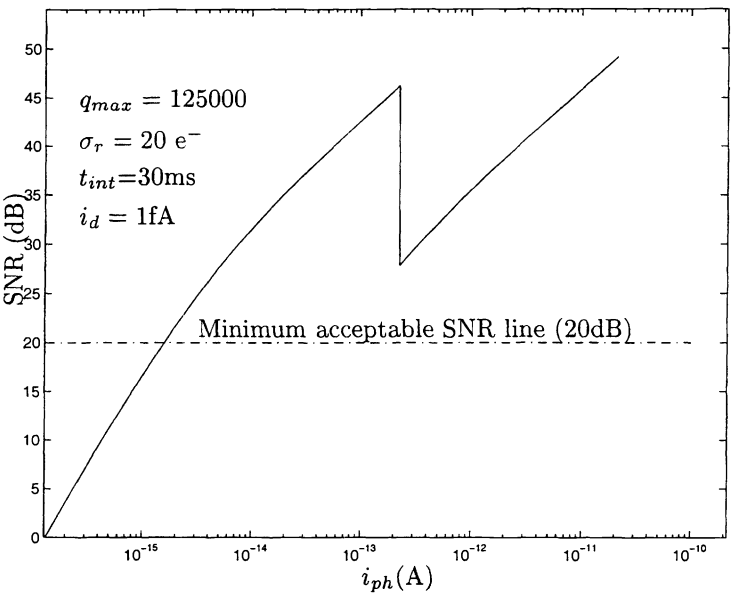


**Figure 20.** SNR vs. $i_{ph}$ for the well capacity adjustment scheme. Dynamic range is enhanced by a factor of 32


2. M. Sayag, "Non-linear Photosite Response in CCD Imagers." U.S Patent No. 5,055,667, 1991. Filed 1990.
3. T. Nakamura and K. Saitoh, "Recent Progress of CMD Imaging," in *1997 IEEE Workshop on Charge Coupled Devices and Advanced Image Sensors*, June 1997.
4. O. Yadid-Pecht and E. Fossum, "Wide Intrascene Dynamic Range CMOS APS Using Dual Sampling," in *1997 IEEE Workshop on Charge Coupled Devices and Advanced Image Sensors*, June 1997.
5. D. Yang, A. El Gamal, B. Fowler, and H. Tian, "A 640×512 CMOS Image Sensor with Ultra Wide Dynamic Range Floating Point Pixel Level ADC," in *ISSCC Digest of Technical Papers*, (San Fransisco, CA), February 1999. Submitted to ISSCC99.
6. S. Chen and R. Ginosar, "Adaptive Sensitivity CCD Image Sensor," in *Proc. SPIE*, vol. 2415, pp. 303–309, (San Jose, California), February 1995.
7. C. Mead, *Analog VLSI and Neural Systems*, Addison Wesley, 1989.
8. N. Ricquier and B. Dierickx, "Active Pixel CMOS Image Sensor with On-Chip Non-Uniformity Correction," in *1995 IEEE Workshop on Charge Coupled Devices and Advanced Image Sensors*, April 1995.
9. R. V. D. Plassche, *Integrated Analog-to-Digital and Digital-to-Analog Converters*, Kluwer Academic Publishers, 1994.
10. S. Decker, R. McGrath, K. Brehmer, and C. Sodini, "A 256x256 CMOS imaging array with wide dynamic range pixels and column-parallel digital output," in *ISSCC Digest of Technical Papers*, pp. 176–177, (San Fransisco, CA), February 1998.